J. Fluid Mech. (1999), *vol.* 389, *pp.* 27–54. Printed in the United Kingdom

Turbulent fountains in a confined stratified environment

By LYNN J. BLOOMFIELD AND ROSS C. KERR

Research School of Earth Sciences, The Australian National University, Canberra, ACT 0200, Australia

(Received 27 April 1998 and in revised form 10 December 1998)

An experimental and theoretical investigation of the flow and density distribution arising from the upward turbulent injection of a dense fluid into a stratified environment of finite extent is presented. Initially, the rising fluid reaches a maximum height before the flow reverses direction and intrudes either along the base of the tank or at an intermediate height in the environment. As more dense fluid is added through either a point or line source, both the fountain and the environment evolve with time. We determine expressions for the motion of the ascending and descending 'fronts' that mark the vertical extent of the spreading layer. We also consider the changes to the environmental density profile and determine an expression for the rate at which the top of the fountain rises due to these changes. Finally, we apply our results quantitatively to two physical problems: the replenishment of magma chambers and the heating or cooling of a room.

1. Introduction

Turbulent fountains and plumes arise in a variety of environments, ranging from large magma chambers in the Earth's crust, to the interior of buildings, and to the Earth's oceans and atmosphere. In all of these examples, both the flow and environment evolve with time as the presence of confining boundaries results in the accumulation of injected fluid. As a result, previous investigations of fountains and plumes have been aimed at understanding both the initial flow and the evolution of the flow and environment in a region of finite extent (see table 1).

The continuous flow of a plume into a confined region containing an initially homogeneous fluid was first analysed by Baines & Turner (1969). They determined the changes to the environmental density profile resulting from the continuous addition of buoyant fluid from both point and line sources. This problem subsequently became known as a 'plume filling box' model. Similar filling box models have since been applied to axisymmetric plumes in an initially stratified fluid (Cardoso & Woods 1993) and to fountains in initially homogeneous surroundings (Baines, Turner & Campbell 1990).

The 'fountain filling box' models developed by Baines *et al.* (1990) describe the flow of a dense fluid injected into a confined homogeneous region through both axisymmetric and line sources. The initial flow of an axisymmetric fountain was first described by Turner (1966), where the injected fluid reaches an initial height before falling to the base of the tank and spreading as a thin layer. As the flow continues, however, more dense fluid reaches the base of the tank causing the layer to increase in thickness as the presence of the tank walls restricts the lateral spreading. Baines *et*

Environment	Plumes	Fountains
Unconfined homogeneous	Morton *et al.* (1956)	Morton (1959); Turner (1966)
Unconfined stratified	Morton *et al.* (1956)	Morton (1959); Bloomfield & Kerr (1998)
Confined homogeneous	Baines & Turner (1969)	Baines, Turner & Campbell (1990)
Confined stratified	Cardoso & Woods (1992)	This study

TABLE 1. Some major contributions to the study of turbulent fountains and plumes.

al. (1990) developed expressions to quantify the motion of the *ascending front* which marks the top of the layer, the changes to the ambient density profile and the rise of the fountain height as a result of these changes.

More recently, Bloomfield & Kerr (1998) have examined the initial flow of a fountain in a stratified fluid. In particular, they found that the strength of the stratification determines whether the falling fluid spreads along the base of the tank or intrudes at an intermediate height in the environment. In this paper, we aim to develop 'stratified filling box' models to quantify the subsequent evolution of the fountain and the environment when either basal or intermediate spreading occurs.

In § 2, we describe experimental observations of the flow from both axisymmetric and line sources. Theoretical predictions of the time evolution of the fountain and the ambient density profile are developed for axisymmetric fountains in § 3. These predictions are then compared to experimental results under a range of different conditions. A similar analysis for line fountains is then presented in § 4. Some illustrative examples of the applications of these results to the replenishment of magma chambers and to the heating or cooling of a room are discussed quantitatively in § 5. Finally in §6 we present our conclusions and summarize the main results.

2. Qualitative observations

Axisymmetric fountains are produced in the laboratory by injecting dense fluid upwards through a nozzle placed on the base of a tank containing stably stratified fluid of lower density. The dense source fluid rises until the effect of gravity brings it to rest at an initial height. This height is then reduced to a final value as the flow reverses direction and the downflow interacts with the continued upflow. The entrainment of lighter ambient fluid reduces the density of the fluid in the fountain. Depending on the extent of this change in density, the downflow either spreads along the base of the tank or intrudes at an intermediate height (Bloomfield & Kerr 1998).

In a homogeneous environment, the falling fluid reaches the base of the tank where it spreads as a thin layer until restricted by the walls (Baines *et al.* 1990). The top of the layer represents a density discontinuity in the environment, and this ascending front rises as ambient fluid from above it is entrained into the downflow. As the layer increases in thickness, the dense fluid that has accumulated below the front is re-entrained back into the downflow of the fountain. Consequently, all subsequent fluid arrives at the base of the tank even denser, and a weak, stable density gradient is established in the environment below the front. The presence of the dense layer reduces the density difference between the source fluid and its immediate environment, and thus causes the fountain height to rise. However, the ascending front rises faster than the fountain height, so that, eventually, it overtakes the top of the fountain.

After this point, the fountain interacts only with the stratified layer, and the rise of the front is controlled only by the rate at which source fluid is added.

In a weakly stratified environment with a sufficiently large buoyancy flux at the source, the downflow still spreads along the base (Bloomfield & Kerr 1998) and the subsequent behaviour is qualitatively similar to that observed in a homogeneous environment. However, as the stratification increases and the buoyancy flux at the source decreases, the spreading height rises from the base of the tank (figure 1*a*). In this situation, the qualitative behaviour of the fountain height and the ascending front remain unchanged from that observed in a homogeneous fluid (figure 1*b*, *c*). However, an additional *descending front* at the bottom of the spreading layer moves towards the base of the tank (figure 1*b*) as fluid from below it is entrained into the upflow of the fountain. The formation of a second front in a stratified fluid is analogous to the 'plume filling box' models in which one front is observed in a homogeneous environment (Baines & Turner 1969) while two form in a stratified fluid (Cardoso & Woods 1993).

When intermediate intrusion occurs, the changes to the ambient density profile also contrast with those observed in an initially homogeneous fluid. The initial density of the intruding layer is equal to that in the environment at the spreading height, so that the environmental density profile is not significantly altered by the first, thin outflow. Subsequent fluid which re-entrains this new layer therefore arrives at the spreading height with approximately the same density. Consequently, the fountain effectively homogenizes the initially stratified ambient fluid.

Similar qualitative behaviour is observed in line fountains. After rising to an initial height, the flow reverses direction to fall on either side of the upflow. In a homogeneous environment, the falling fluid spreads along the base of the tank forming an ascending front above a stratified layer (Baines *et al.* 1990). As the initial ambient density gradient increases, the spreading height rises from the base and both ascending and descending fronts bounding a nearly homogeneous layer are observed (figure 2*a*). However, during random periods, an instability in the flow causes the downflow to be deflected to one side of the upflow, momentarily decreasing the fountain height (figure 2*b*). The frequency of these fluctuations in the profile decreases as the ambient stratification increases. In an initially stratified fluid, therefore, the fountain profile remains predominantly symmetric until the homogenization of the environment results in more frequent fluctuations.

3. Axisymmetric fountains

The investigation of axisymmetric fountains proceeds as follows. We begin by describing the experimental apparatus and methods in § 3.1. In § 3.2 we briefly review the initial fountain behaviour in an effectively infinite environment. We then proceed in § 3.3 to analyse the flow in a confined environment, and the predicted results for the fronts and the fountain height are compared with the experimental data. Finally, in § 3.4, we develop a simple numerical model of the changes in the ambient density profile with time, which is compared with our experimental measurements.

3.1. *Experimental methods*

The experiments were carried out in an acrylic tank which was 38 cm × 38 cm in internal cross-section and 80 cm deep. The ambient linear density gradient, of approximately 25 cm depth, was established with NaCl solutions using the double

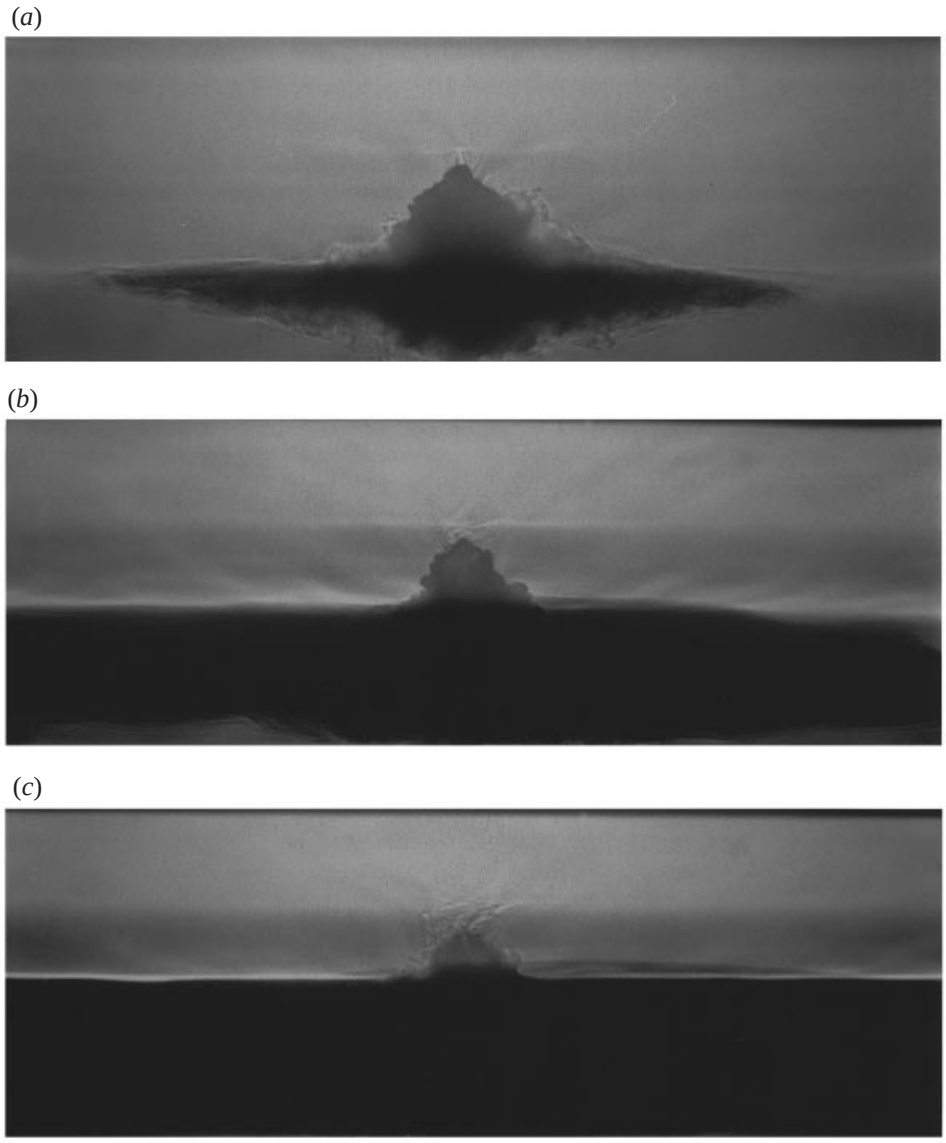

FIGURE 1. Photographs of an axisymmetric fountain with $Q_o = 4.5 \times 10^{-5}\,\mathrm{m^3\,s^{-1}}$, $N = 1.7\,\mathrm{s^{-1}}$ and $\Delta_o = 0$. (*a*) When intermediate intrusion occurs, both ascending and descending fronts are observed ($t = 23$ s). As the flow continues, (*b*), the descending front reaches the base of the tank ($t = 2$ min), while in (*c*) the ascending front approaches the top of the fountain ($t = 3$ min 30 s).

bucket method (Oster 1965). The fluid densities were measured by refractometry to within 0.1%, giving a relative error in the density gradient of approximately 1%.

The source fluid was placed in a 20 l bucket which was raised 1.5 m higher than the main tank. The flow rate resulting from this gravitational head, which was kept constant throughout an experiment, was measured with a flow meter to an accuracy of 2–3%. The source fluid was injected upwards from the base of the tank through a tube with an 8.8 mm inner diameter. Two sets of cross-hairs of 0.5 mm diameter were positioned 3 mm and a further 44 mm from the tube outlet to ensure that the flow

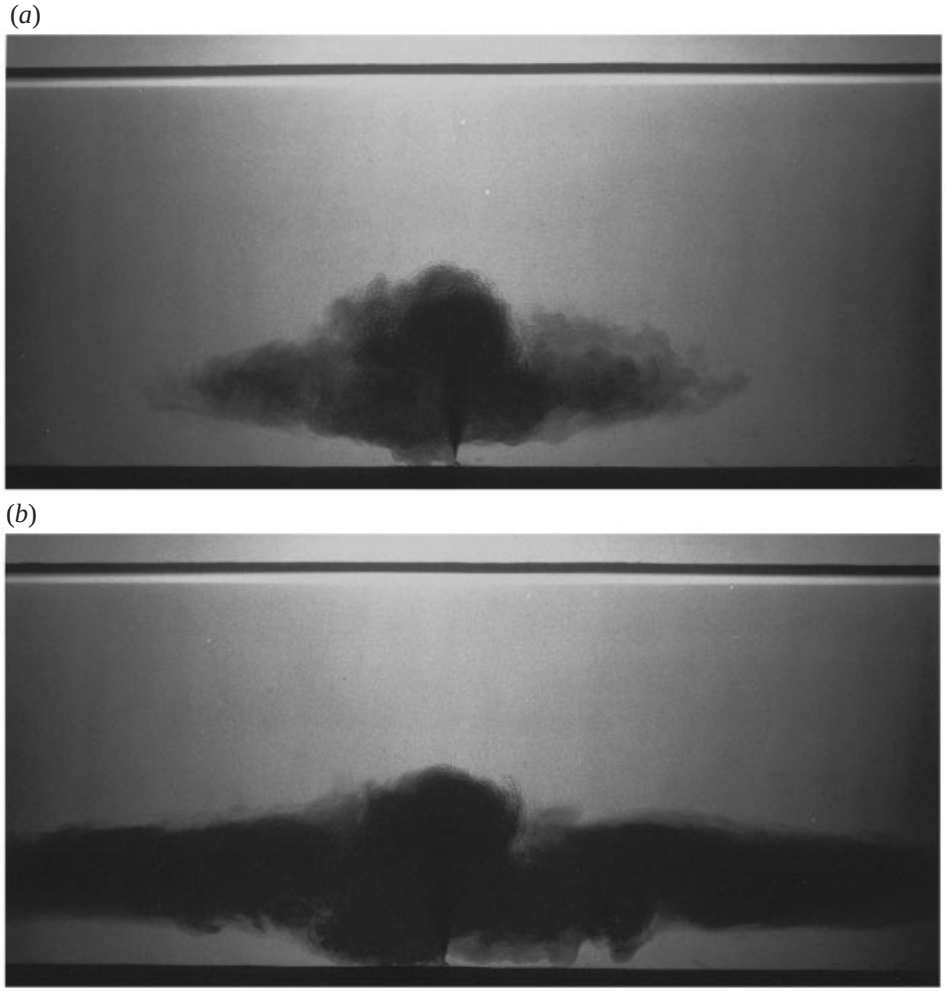

FIGURE 2. Photographs of a line fountain in which $q_o = 8.8 \times 10^{-5}\,\mathrm{m^2\,s^{-1}}$, $N = 0.75\ \mathrm{s^{-1}}$ and $\Delta_o = 0$. (*a*) Intermediate intrusion again leads to the formation of two fronts ($t = 21$ s). (*b*) During random intervals, the downflow is deflected to one side of the upflow ($t = 47$ s).

was turbulent from the source (Bloomfield & Kerr 1998). Using a method outlined by Baines *et al.* (1990), measurements of the position of the descending front formed by a weakly buoyant jet indicated that the position of the virtual point source was a distance $z_v = 1.0 \pm 0.2$ cm below the base of the tank, and the effective source radius was $r_e = 4.16 \pm 0.23$ mm (Bloomfield & Kerr 1998).

The flows were observed using the shadowgraph method, and dye was introduced into the input fluid to mark the extent of the spreading layer. Recording the flows on video enabled the mean fountain height to be measured to within 0.5 cm, or 2–4%.

The density profile was measured during the experiment by stopping the flow and withdrawing samples from a range of depths. The densities of these samples were then measured by refractometry. It was observed that stopping and starting the flow did not disturb the position of the fronts.

3.2. *The initial flow in an infinite environment*

During the first stages of the flow in a stratified fluid, the initial, final and spreading heights of the fountain are given by the expressions developed by Bloomfield & Kerr (1998) for the flow in an infinite environment. These heights were found by a dimensional argument to be

$$z = f(\sigma) M_o^{3/4} F_o^{-1/2}, \tag{3.1}$$

where the dimensionless parameter, σ, is defined by $\sigma = M_o^2 N^2 / F_o^2$, $\rho_i M_o = Q_o^2/(\pi r_e^2)$ is the momentum flux at the source, $\rho_i F_o = \rho_i \Delta_o Q_o$ is the buoyancy flux at the source and $N^2 = -(g/\rho_o)(\mathrm{d}\rho/dz)$ is the square of the buoyancy frequency. In these expressions, Q_o is the volume flux at the source, $\Delta_o = g(\rho_i - \rho_o)/\rho_o$, g is the gravitational acceleration, z is the height above the source and ρ is the ambient fluid density, with ρ_o the density at the base of the tank and ρ_i the density of the input fluid. By combining their experimental results with those of Baines *et al.* (1990), it was found by Bloomfield & Kerr (1998) that in the limits of small and large σ, the appropriate $f(\sigma)$ for the initial, final and spreading heights, respectively, are given by

$$f_i(\sigma) = \begin{cases} 2.65, & \sigma < 0.1 \\ 3.25\sigma^{-1/4}, & \sigma > 40, \end{cases} \tag{3.2a}$$

$$f_f(\sigma) = \begin{cases} 1.85, & \sigma < 0.1 \\ 3.00\sigma^{-1/4}, & \sigma > 40, \end{cases} \tag{3.2b}$$

and

$$f_s(\sigma) = \begin{cases} 0, & \sigma < 5 \\ 1.53\sigma^{-1/4}, & \sigma > 40. \end{cases} \tag{3.2c}$$

For all values of σ, the simple functions

$$f_i(\sigma) = \left(2.65^{-4} + 3.25^{-4}\sigma\right)^{-1/4} \tag{3.3a}$$

and

$$f_f(\sigma) = \left(1.85^{-4} + 3.0^{-4}\sigma\right)^{-1/4} \tag{3.3b}$$

are a good fit to the experimental results (figure 3).

3.3. *The motion of the fronts*

To quantify the motion of the fronts, we make the simplifying assumption that the intruding fluid spreads instantaneously as a thin layer at the height of neutral buoyancy. In Appendix A we show that the assumption of instantaneous spreading is a reasonable approximation, as the timescale of the intrusion is only a small fraction of that of the vertical flow in the environment. The qualitative observation is also made that, as the radial distance increases, the thickness of the outflow quickly becomes small compared to the spreading height. These calculations and observations combine to allow us to ignore the dynamics of the spreading layer in the following analysis.

3.3.1. *The descending front*

The motion of the descending front can be found by writing the equation for the conservation of volume flux in the region below the front. Hence, if the cross-sectional area of the tank, A, is much greater than that of the fountain,

$$A\frac{\mathrm{d}z_d}{\mathrm{d}t} = -Q_d, \tag{3.4}$$

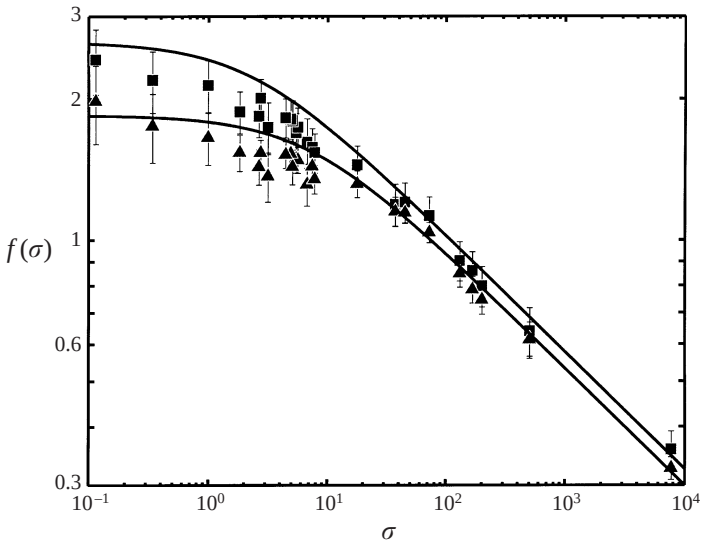

FIGURE 3. Experimental measurements of the initial (■) and final (▲) fountain heights as a function of σ. Also shown are the analytical functions given in (3.3) for the initial and final heights respectively.

where $z_d(t)$ is the height of the front above the virtual point source and Q_d is the volume flux of fluid entrained into the fountain from below z_d. An expression for the total volume flux in the upflow of the fountain, $Q(z)$, can be found from a solution of the entrainment equations. These equations, which describe the conservation of volume, $b^2\omega$, momentum, $b^2\omega^2$, and buoyancy, $b^2\omega\Delta$, are (Turner 1973)

$$\frac{\mathrm{d}}{\mathrm{d}z}(b^2\omega) = 2\alpha b\omega, \quad \frac{\mathrm{d}}{\mathrm{d}z}(b^2\omega^2) = b^2\Delta, \quad \frac{\mathrm{d}}{\mathrm{d}z}(b^2\omega\Delta) = -b^2\omega N^2, \tag{3.5}$$

where α is the entrainment coefficient, b is the fountain radius, ω is the axial fluid velocity, and Δ is the buoyant acceleration of the fountain fluid. Equations (3.5) were solved for the flow through the actual source ($Q_o \neq 0$) with Q_o, Δ_o and N^2 varied over the range of experimental values. The solutions for the volume flux were then compared with the corresponding result for a jet ($F_o = 0$, $N^2 = 0$) showing, in all cases, a difference of less than 1% at the respective spreading heights (see figure 4 for the $\sigma = \infty$ results). For all values of σ, therefore, the volume flux in the upflow of the fountain can be approximated by the corresponding result for a jet. An analytical solution of (3.5) for a jet, which satisfies the boundary conditions at the actual source gives

$$Q(z) = 2\alpha Q_o \frac{z - z_v}{r_e} + Q_o, \tag{3.6}$$

where $\alpha = 0.076 \pm 0.004$ (Rodi 1982). Whenever intermediate intrusion occurs, therefore, the entrained volume flux between z_v and z_d is

$$Q_d = 2\alpha Q_o \frac{z_d - z_v}{r_e}. \tag{3.7}$$

To simplify this and subsequent expressions, we introduce the dimensionless heights, $\tilde{z}$, and times, $\tilde{t}$, defined by

$$\tilde{z} = \frac{z}{r_e} \quad \text{and} \quad \tilde{t} = \frac{Q_o t}{A r_e}. \tag{3.8}$$

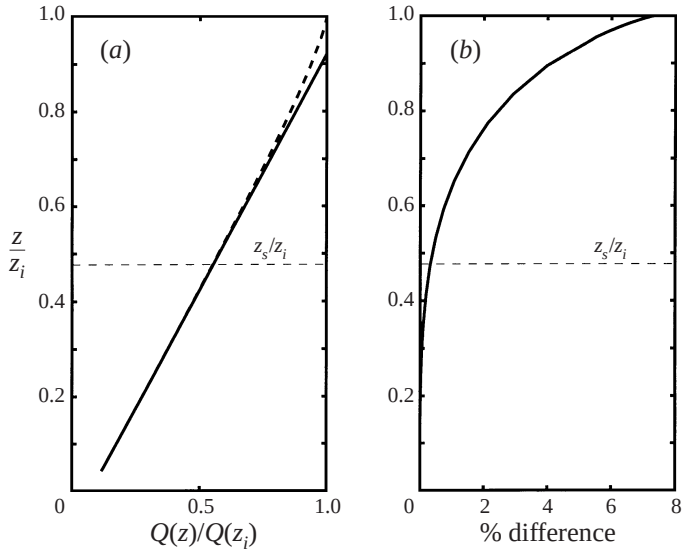

FIGURE 4. (*a*) Comparison between the volume flux in an axisymmetric jet in both homogeneous (solid line) and stratified (broken line) surroundings in which $\sigma = \infty$, with (*b*) showing the small difference in regions below the spreading height.

With the use of (3.7) and (3.8), (3.4) is integrated to give a solution for the height of the descending front above the base of the tank:

$$(\tilde{z}_d - \tilde{z}_v) = (\tilde{z}_s - \tilde{z}_v)\mathrm{e}^{-2\alpha\tilde{t}}, \tag{3.9}$$

where $\tilde{z}_s$ is the dimensionless spreading height.

This exponential decrease in the height of the descending front contrasts with the algebraic decrease in the height of the descending fronts formed by an axisymmetric plume in either a homogeneous (Baines & Turner 1969) or a stratified fluid (Cardoso & Woods 1993).

3.3.2. *The ascending front*

The motion of the ascending front, $z_a(t)$, is determined by writing the expression for the conservation of volume flux at the level of the front. Thus

$$A\frac{\mathrm{d}z_a}{\mathrm{d}t} = Q_o + Q_a, \tag{3.10}$$

where Q_a is the volume flux of ambient fluid entrained into the downflow from above the front. Baines *et al.* (1990) described some experimental measurements made by T. J. Reedman which indicated that, in a homogeneous fluid, the entrained volume flux per unit height into the downflow of the fountain is constant and is given by

$$\frac{\mathrm{d}Q_a}{\mathrm{d}z} = B\frac{Q_o}{r_e}, \tag{3.11}$$

where B was found experimentally to be $B \approx 0.25$. Baines *et al.* (1990) also explained that the observation of constant entrainment per unit height can be understood by viewing the downflow as a line plume which encircles the upflow. In a linearly stratified environment, the behaviour of a plume is little different to that in a uniform fluid until close to the spreading height (Turner 1973; Cardoso & Woods 1993). As a

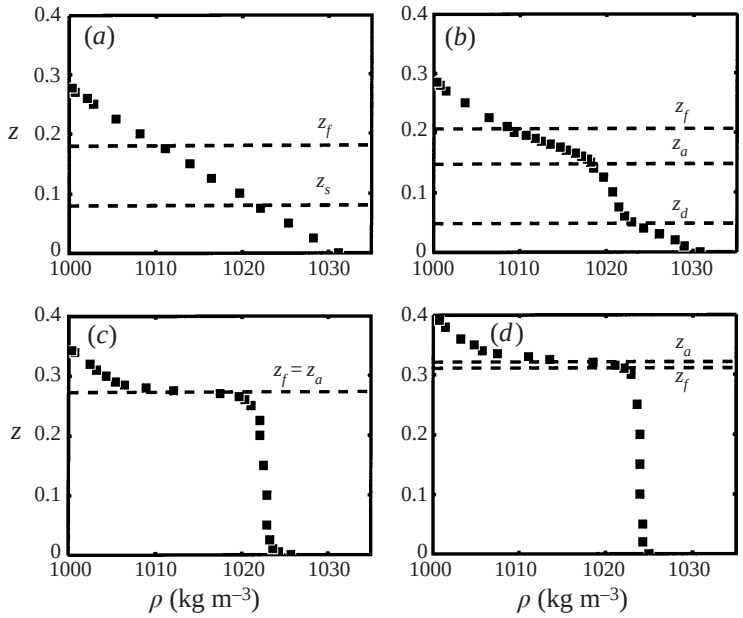

FIGURE 5. Experimental measurements of the changing ambient density profile produced by an axisymmetric fountain with $Q_o = 3.04 \times 10^{-5}\,\mathrm{m^3\,s^{-1}}$, $N = 1.03\,\mathrm{s^{-1}}$ and $\Delta_o = 0$. Profiles were measured at (*a*) $t = 0$ s, (*b*) $t = 46$ s, (*c*) $t = 5$ min 32 s and (*d*) $t = 9$ min 34 s.

result, (3.11) also accurately predicts the entrainment into the downflow of a fountain in a stratified fluid. The total volume flux entrained between $\tilde{z}_a$ and $\tilde{z}_f$ is therefore

$$Q_a = \frac{BQ_o}{r_e}(z_f - z_a). \tag{3.12}$$

Using (3.8), and introducing (3.12) into (3.10), leads to the general result that

$$\frac{\mathrm{d}\tilde{z}_a}{\mathrm{d}\tilde{t}} = 1 + B(\tilde{z}_f - \tilde{z}_a). \tag{3.13}$$

This result is independent of the environmental conditions and so applies for all values of σ.

After the ascending front has reached the top of the fountain at a time t^*, the position of the front rises at the same rate as the free surface rises due to the addition of fluid to the tank, so that $\mathrm{d}\tilde{z}_a/\mathrm{d}\tilde{t} = 1$. To integrate (3.13) for times $t < t^*$, we need an expression for the increase in the fountain height with time.

3.3.3. *The fountain height*

In developing an expression for the fountain height, we must take into account two separate effects. As discussed in § 2 and shown quantitatively in figure 5, the fountain effectively homogenizes the initially stratified environment, while the addition of dense source fluid increases the average ambient density. The environment of the fountain quickly becomes mixed so that at small times (figure 5*b*), the decrease in the average ambient density gradient over the height of the fountain is a more significant effect than the increase in the average density. At large times, when the environment is nearly homogeneous (figure 5*c*, *d*), the opposite is true. To determine the contribution from each of these effects, we derive two expressions for the fountain height: $z_{fs}(t)$,

which gives the rise due to the decreasing stratification, and $z_{fh}(t)$, which is based on the results of Baines *et al.* (1990) for a fountain in a homogeneous fluid of increasing density. The detailed derivation of these expressions, which is shown in Appendix B, gives the result that:

$$\tilde{z}_{fs} = \tilde{z}_{fs}(0) + \frac{3.0^{-4}\sigma_o}{1.85^{-4} + 3.0^{-4}\sigma_o}\frac{\tilde{z}_{rs}}{4}\tilde{t}, \tag{3.14a}$$

and

$$\tilde{z}_{fh} = \tilde{z}_{fh}(0) + \tfrac{1}{2}\tilde{z}_{rh}\tilde{t}, \tag{3.14b}$$

where $\tilde{z}_{fs}(0)$ is the height of the fountain at $\tilde{t} = 0$, σ_o is the measured value of σ at $t = 0$, $\tilde{z}_{rs} = \tilde{z}_{fs}(0)/(\tilde{z}_{fs}(0) - \tilde{z}_v)$, $\tilde{z}_{rh} = \tilde{z}_{fh}(0)/(\tilde{z}_{fh}(0) - \tilde{z}_v)$, and $\tilde{z}_{fh}(0)$ is defined in (B 9).

To quantify the fountain height at all times, we combine (3.14*a*) and (3.14*b*) into a single expression for the fountain height which characterizes the transition from $\tilde{z}_{fs}$ at small times to $\tilde{z}_{fh}$ as $\tilde{t} \to \tilde{t}^*$. A suitable expression for $\tilde{z}_f(\tilde{t})$ is therefore

$$\tilde{z}_f(\tilde{t}) = (1 - w(\tilde{t}))\tilde{z}_{fs} + w(\tilde{t})\tilde{z}_{fh}, \tag{3.15}$$

where $w(\tilde{t})$ is a function which is equal to 0 at $\tilde{t} = 0$ and becomes equal to 1 at $\tilde{t} = \tilde{t}^*$. A simple weighting function which quantifies the fraction of fluid below $\tilde{z}_f$ which is homogeneous, and therefore satisfies the required limits, is given by

$$w = \frac{\tilde{z}_a - \tilde{z}_d}{\tilde{z}_f - \tilde{z}_v}. \tag{3.16}$$

Introducing (3.16) into (3.15) and solving for $\tilde{z}_f$ gives a final expression for the fountain height:

$$\tilde{z}_f = \tfrac{1}{2}\left(\tilde{z}_{fs} + \tilde{z}_v\right) + \left(\tfrac{1}{4}\left(\tilde{z}_{fs} + \tilde{z}_v\right)^2 + \left(\tilde{z}_a - \tilde{z}_d\right)\left(\tilde{z}_{fh} - \tilde{z}_{fs}\right) - \tilde{z}_v\tilde{z}_{fs}\right)^{1/2}. \tag{3.17}$$

This expression can then be used in the numerical integration of (3.13) to give a solution for the ascending front. Finally, from this result for $\tilde{z}_a$, the position of the fountain height can be calculated from (3.17).

3.3.4. *Experimental results*

The positions of the fountain height and the fronts were measured in a series of experiments performed for a range of values of σ. The data from three of these experiments are shown in figure 6 along with the result of integrating (3.13) for the ascending front, the predicted position of the fountain height (3.17) and, where applicable, the expression for the descending front (3.9). The fountain height at $\tilde{t} = 0$ was determined from (3.3*b*). The value of z_s was estimated from graphs of previous experimental results for the spreading height plotted against σ (for example, figure 7 in Bloomfield & Kerr 1998). In general, the good agreement between theory and experiment for the fountain height and ascending front indicates that the assumptions made, and the simple weighting function used, describe the actual fountain behaviour well. The experimental results indicate that the descending front falls slightly faster than predicted by (3.9). This faster descent is almost certainly due to the effect of the additional entrainment into the overshooting fluid below the front, which is not included in our model.

3.4. *Ambient density profile*

A simple numerical model based on that developed by Germeles (1979) is used to quantify the changes to the environmental density profile. The initial linear gradient is approximated by thin, discrete layers at heights $\tilde{z}_j$ and with thickness $\Delta\tilde{z}_j = \tilde{z}_{j+1} - \tilde{z}_j$.

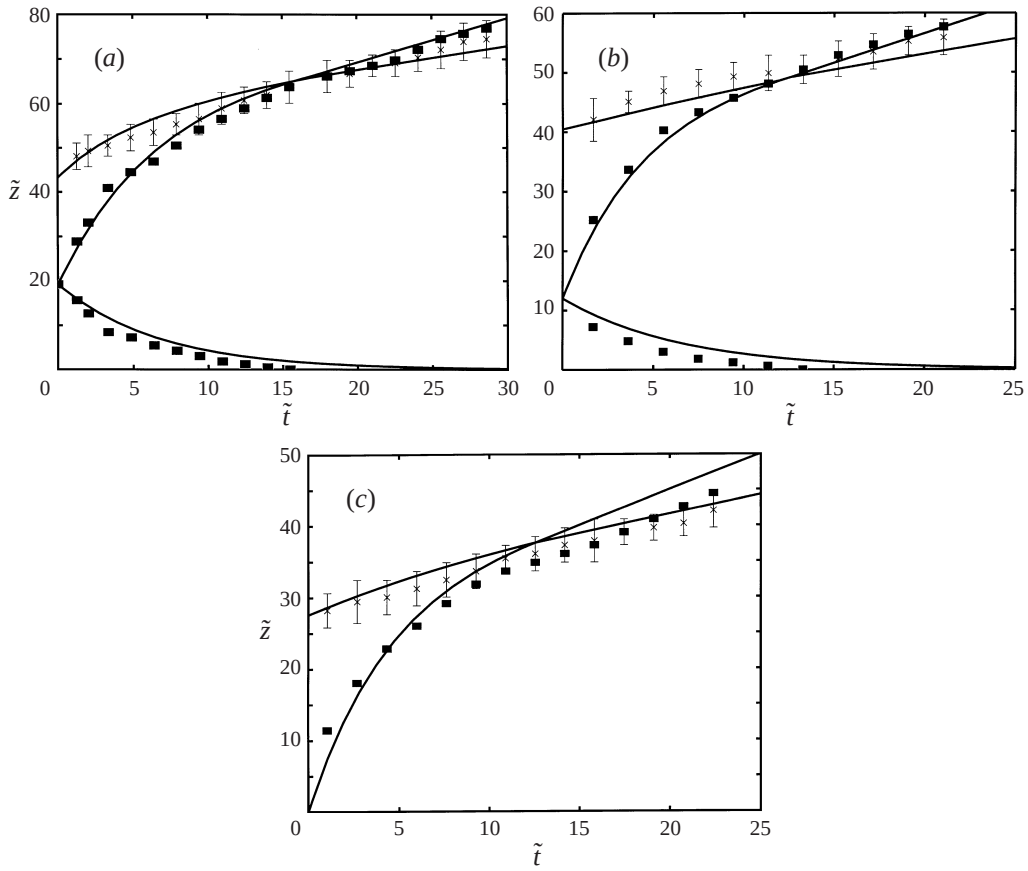

FIGURE 6. The non-dimensional height of the axisymmetric fountain (×) and the positions of the fronts (■), as a function of time, together with the theoretical predictions (solid lines) for the fountain height (3.17), the ascending front (3.13) and, where applicable, the descending front (3.9). The experimental parameters were (*a*) $Q_o = 3.04 \times 10^{-5}\,\mathrm{m^3\,s^{-1}}$, $N = 1.03\,\mathrm{s^{-1}}$; $\sigma = \infty$, (*b*) $Q_o = 3.87 \times 10^{-5}\,\mathrm{m^3 s^{-1}}$, $N = 1.22\,\mathrm{s^{-1}}$, $\Delta_o = 0.23\,\mathrm{m\,s^{-2}}$; $\sigma = 14$, and (*c*) $Q_o = 3.25 \times 10^{-5}\,\mathrm{m^3\,s^{-1}}$, $N = 1.28\,\mathrm{s^{-1}}$, $\Delta_o = 0.37\,\mathrm{m\,s^{-2}}$; $\sigma = 4$.

The decreasing density in successive layers therefore results in a stepped profile. During any small time interval, $\Delta\tilde{t}$, the volume entrained from any of these layers into the upflow or downflow of the fountain can be found using (3.7) or (3.12) respectively. This entrainment causes the thickness of the steps in the profile to be reduced to

$$\Delta\tilde{z}'_j = \Delta\tilde{z}_j - \begin{cases} 2\alpha\Delta\tilde{t}\Delta\tilde{z}_j, & \tilde{z}_j < \tilde{z}_d \\ B\Delta\tilde{t}\Delta\tilde{z}_j, & \tilde{z}_d < \tilde{z}_j < \tilde{z}_f, \end{cases} \tag{3.18}$$

while the density at each step is unchanged. The positions of $\tilde{z}_d$ and $\tilde{z}_f$ in this stepped profile are determined from (3.9) and (3.17), respectively.

The ambient fluid entrained into the fountain in the interval $\Delta\tilde{t}$ mixes with the injected source fluid, so that when the downflow reaches the point of intrusion, the fountain fluid has a density, ρ_m, given by

$$\rho_m(Q_o + Q_e) = \rho_i Q_o + \int_{z_v}^{z_f} \rho(z)\frac{\mathrm{d}Q_e}{\mathrm{d}z}\mathrm{d}z. \tag{3.19}$$

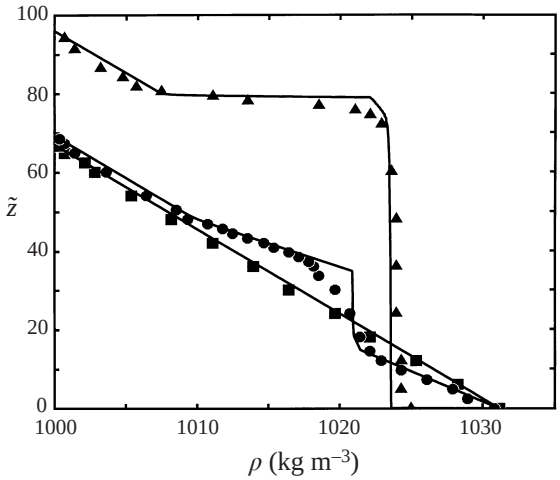

FIGURE 7. Ambient density profiles produced by an axisymmetric fountain, with the experimental parameters listed in the caption to figure 5. The measured profiles at $t = 0$ (■), $t = 46$ s (●) and $t = 9$ min 34 s (▲) are shown in comparison with the numerical prediction (solid line).

For our stepped profile, and in terms of the dimensionless quantities defined in (3.8),

$$\rho_m = \frac{\rho_i + 2\alpha \sum_{\tilde{z}_j=\tilde{z}_v}^{\tilde{z}_d} \rho(\tilde{z}_j)\Delta\tilde{z}_j + B \sum_{\tilde{z}_j=\tilde{z}_d}^{\tilde{z}_f} \rho(\tilde{z}_j)\Delta\tilde{z}_j}{1 + 2\alpha \sum_{\tilde{z}_j=\tilde{z}_v}^{\tilde{z}_d} \Delta\tilde{z}_j + B \sum_{\tilde{z}_j=\tilde{z}_d}^{\tilde{z}_f} \Delta\tilde{z}_j}. \tag{3.20}$$

The fluid with this density then flows laterally into the environment to form a new layer of thickness

$$\Delta\tilde{z}'_n = \left(1 + 2\alpha \sum_{\tilde{z}_j=\tilde{z}_v}^{\tilde{z}_d} \Delta\tilde{z}_j + B \sum_{\tilde{z}_j=\tilde{z}_d}^{\tilde{z}_f} \Delta\tilde{z}_j\right)\Delta\tilde{t}. \tag{3.21}$$

With each time step, therefore, the density profile can be updated to determine how it evolves with time by reducing the thickness of the layers below $\tilde{z}_f$ and adding the new layer at the correct step in the profile.

An example of the result of this procedure is compared to the experimental data in figure 7. The initial step sizes were chosen to be $\Delta z = 1$ mm, while Δt was decreased until $\Delta t = 1$ s, after which further decreases did not change the final result. At small times, the numerical results predict a much more homogeneous spreading layer than that observed experimentally. The additional variation in the densities in the spreading layer most probably arises from a combination of two effects-additional mixing below the descending front, and the fact that the downflow has a range of densities which leads to a range of intrusion heights. At later times, the agreement between the numerical and experimental results is much better, with the numerical results only slightly underestimating the density within the spreading layer.

4. Line fountains

4.1. *Experimental methods*

To investigate the flow from a line source, we used the same tank as was employed previously by Baines *et al.* (1990) and by Bloomfield & Kerr (1998). This acrylic tank, which was 120 cm × 8 cm in internal cross-section and 60 cm deep, was filled to a depth of approximately 40 cm. Two rolls of fly wire placed in the ends of the tank acted as damping screens. These were necessary to prevent the formation of a mixed layer in the environment as a result of the deflection of the spreading layer as it reached the tank walls (Baines *et al.* 1990; Bloomfield & Kerr 1998). The source, which was located centrally on the base of the tank and perpendicular to its length, consisted of a circular pipe of 4 mm inner diameter with 31 holes of 0.6 mm diameter spaced evenly along its length. The initial three-dimensional flow from these holes should coalesce to two-dimensional flow at a height of approximately 1.5 cm above the source (Crapper 1977). This prediction is in agreement with experimental observations, which indicate a transition at 1–2 cm above the outlet of the holes. In order to conserve momentum flux during this transition, the equivalent slot area must be equal to the total effective area of the holes, and therefore depends on the velocity profile at the source. Fully turbulent flow would give an area equal to the total measured area of the holes, resulting in a slot width of 54.8 μm. The corresponding result for laminar flow indicates a slot width of $\frac{5}{6}\times$ 54.8 μm = 45.7 μm. As the momentum flux cannot be measured directly, a value of the effective slot width, b_o, was determined by performing an experiment with a weakly buoyant jet. Assuming a 'top hat' velocity profile in the jet, the elevation of the resulting descending front, z_d, is given by

$$z_d^{1/2} = H^{1/2} - \left(\frac{q_o^2\alpha}{2b_oL^2}\right)^{1/2} t, \tag{4.1}$$

where H is the depth of fluid in the tank, q_o is the volume flux per unit length of the source, $\alpha = 0.074 \pm 0.004$ (Rodi 1982) is the two-dimensional jet entrainment coefficient for a top hat profile and L is the length of the tank (Baines *et al.* 1990; Bloomfield & Kerr 1998). The square root of the measured elevation of the descending front is plotted against time in figure 8, showing the transition from the three-dimensional flow at small heights to the linear relationship in the two-dimensional regime. From the slope of the line, the effective slot width was determined to be $b_o = 46.5 \pm 2.2$ μm. This value indicates that the flow is virtually laminar at the source for the flow rates of $q_o = (2-2.2)\times 10^{-4}\ \mathrm{m^2\,s^{-1}}$ used in these experiments. The virtual source was determined to coincide with the top of the nozzle, so that all heights in this and subsequent experiments were measured above the outlet of the holes, which were located a distance of $z_e = 1.4$ cm above the base of the tank.

4.2. *The initial flow in an infinite environment*

Expressions for the initial, final (symmetric and asymmetric) and spreading heights of a line fountain in an infinite environment were found by Bloomfield & Kerr (1998) to be given by

$$z = f(\sigma^*)m_o f_o^{-2/3} \tag{4.2}$$

where the dimensionless parameter, σ^*, is defined by $\sigma^* = m_o^2N^2/f_o^2$, $\rho_i m_o = q_o^2/(2b_o)$ is the initial momentum flux per unit length and $\rho_i f_o = \rho_i \Delta_o q_o$ is the initial buoyancy flux per unit length of the source.

Since the rise in the ascending front is very sensitive to the fountain height, we

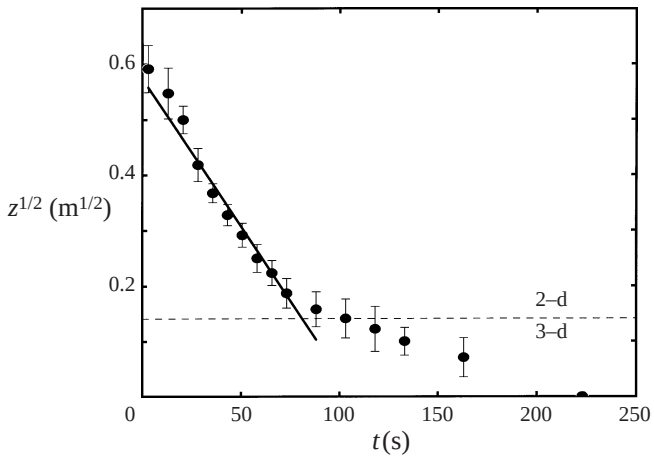

FIGURE 8. Elevation of the descending front formed by a line jet with $q_o = 2.2 \times 10^{-4}$ m^2 s^{-1}, showing the transition from three-dimensional flow to two-dimensional flow at a height of 2 cm above the source. From the slope of the solid line, the effective slot width was found to be $b_o = 46.5 \pm 2.2$ μm.

performed twelve experiments to examine the function $f(\sigma^*)$ at small values of σ^*. For $\sigma^* = 0$, our results are shown in figure 9. For the symmetric steady height, we obtained a value of 0.95, not 1.3 as determined by Baines *et al.* (1990) and used by Bloomfield & Kerr (1998). This discrepancy, and the corresponding differences in values for the initial and asymmetric heights, are believed to be due to Baines *et al.* (1990) using the external tank width to quantify q_o. When the corrections for the tank width are made, the results of Baines *et al.* (1990) agree, to within experimental errors, with those determined here.

In addition, in our new experiments for small values of σ^*, the fountain heights were found to be lower than those reported by Bloomfield & Kerr (1998). The measurements reported in that study were of small fountains in which the flow was observed to be axisymmetric for approximately 60% of the fountain heights. In contrast, in our new experiments, the fountains were three times higher and the source had twice as many holes. As a result, the flow in these fountains was axisymmetric only over the lower 10% of the fountain height, and therefore should give an accurate estimate of the height of a line fountain.

Figures 12(*a*) and 12(*b*) from Bloomfield & Kerr (1998) are replotted in figure 10 using the new asymptotic limits for a fountain in a homogeneous fluid. From these new graphs, we find that in the limit of small and large σ^*,

$$f_i(\sigma^*) = \begin{cases} 1.26, & \sigma^* < 0.6 \\ 2.46\sigma^{*-1/3}, & \sigma^* > 30, \end{cases} \tag{4.3a}$$

$$f_f(\sigma^*) = \begin{cases} \begin{cases} 0.95, & \sigma^* < 1.0 \\ 2.43\sigma^{*-1/3}, & \sigma^* > 100, \end{cases} & \text{(symmetric)} \\ \begin{cases} 0.72, & \sigma^* < 1.0 \\ 2.27\sigma^{*-1/3}, & \sigma^* > 100, \end{cases} & \text{(asymmetric)} \end{cases} \tag{4.3b}$$

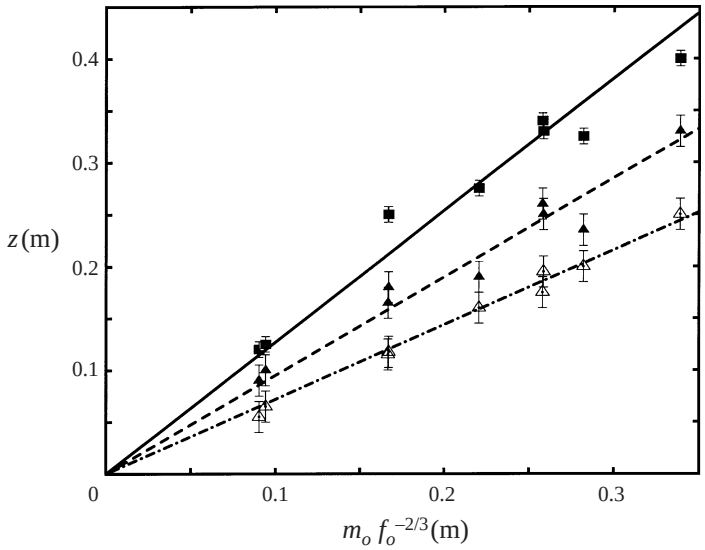

FIGURE 9. Experimental measurements of the initial (■), final symmetric (▲) and final asymmetric (△) fountain heights in a homogeneous fluid. The constant slopes of the lines for the three heights are found to be 1.26 ± 0.08 for the initial height, 0.95 ± 0.05 for the final symmetric height and 0.72 ± 0.02 for the final asymmetric height.

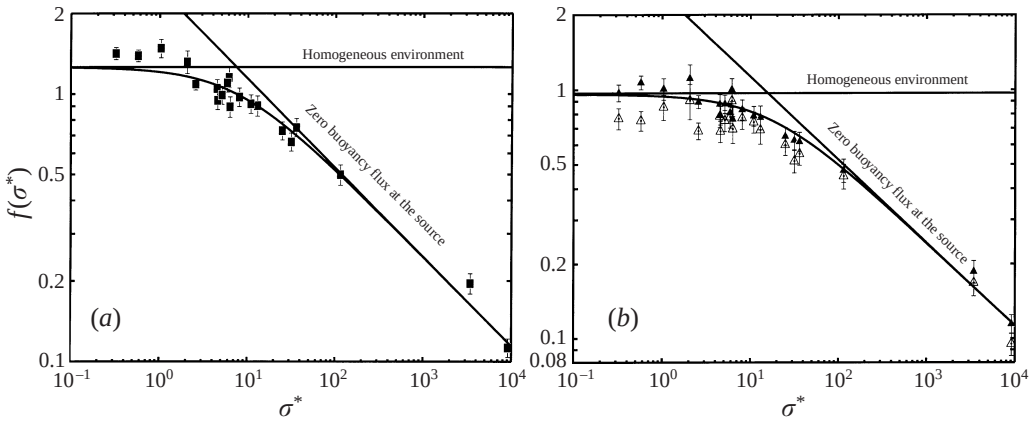

FIGURE 10. Measured heights of a two-dimensional fountain with our new asymptotic results and the simple analytical $f(\sigma)$ given in (4.4). (*a*) Initial height: as $\sigma^* \to 0$, $f(\sigma^*) \to 1.25$ and as $\sigma^* \to \infty$, $f(\sigma^*) \to 2.46\sigma^{*-1/3}$. (*b*) Symmetric (▲) and asymmetric (△) final height with the asymptotic results and $f(\sigma)$ for the symmetric height: as $\sigma^* \to 0$, $f(\sigma^*) \to 0.95$, and as $\sigma^* \to \infty$, $f(\sigma^*) \to 2.43\sigma^{*-1/3}$.

and

$$f_s(\sigma^*) = \begin{cases} 0, & \sigma^* < 6 \\ 1.07\sigma^{*-1/3}, & \sigma^* > 100, \end{cases} \tag{4.3c}$$

for the initial, final and spreading heights, respectively. The experimental results slightly overestimate the predicted asymptotic limit as $\sigma^* \to 0$, with this difference being more significant for the initial fountain height. Also plotted in figure 10 are the two simple functions

$$f_i(\sigma^*) = \left(1.26^{-3} + 2.46^{-3}\sigma^*\right)^{-1/3} \tag{4.4a}$$

and

$$f_f(\sigma^*) = \left(0.95^{-3} + 2.43^{-3}\sigma^*\right)^{-1/3} \tag{4.4b}$$

which approximate the initial and final symmetric heights of a line fountain over the entire range of values of σ^*.

4.3. *The motion of the fronts and experimental results*

Our analysis of line fountains again uses the assumptions that the intruding layer spreads instantaneously as a thin layer at the height of neutral buoyancy. In this case, however, the calculations in Appendix A indicate that the timescale of the lateral outflow is a significant fraction of the time taken for the descending front to reach the base of the tank. At small times, therefore, the dynamics of the outflow may affect the motion of the descending front in particular.

An additional complication arises in line fountains due to the oscillations in the fountain profile, which increase in frequency as the environment is homogenized. As time progresses through an experiment, therefore, these fluctuations will have a more significant effect on the overall evolution of the fountain height and the ascending front.

4.3.1. *The motion of the fronts*

Using those arguments presented in § 3.3.1, we again assume that in our stratified fluid, the upflow remains jet-like for a significant distance above the source. In terms of the dimensionless parameters defined by

$$\tilde{z} = \frac{z}{b_o} \quad \text{and} \quad \tilde{t} = \frac{q_o t}{L b_o}, \tag{4.5}$$

(4.1) becomes

$$\tilde{z}_d^{1/2} = \tilde{z}_s^{1/2} - \left(\frac{\alpha}{2}\right)^{1/2} \tilde{t}. \tag{4.6}$$

The descending front formed by a line fountain should therefore reach the level of the source after a time $\tilde{t}_d = (2\tilde{z}_s/\alpha)^{1/2}$. This result clearly contrasts with that for both axisymmetric fountains and plumes in stratified fluids, where the descending front only asymptotically approaches the level of the source.

The motion of the ascending front is again determined by the conservation of volume flux at the level of the front. Thus

$$L\frac{\mathrm{d}z_a}{\mathrm{d}t} = q_o + q_a, \tag{4.7}$$

where q_a is the total volume flux per unit length entrained into the downflow between the ascending front and the fountain height.

As a result of the fluctuations in the fountain profile, Baines *et al.* (1990) reported difficulties in finding a satisfactory expression for the entrained volume flux into the downflow. As a result, they made the assumption that q_a has the same dependence on height as the jet-like upflow (Baines *et al.* 1990, equation (43)). This leads to the result that

$$\frac{\mathrm{d}q_a}{\mathrm{d}z} = \frac{Bq_o}{2b_o^{1/2}z^{1/2}}, \tag{4.8}$$

where B was determined experimentally to range between 0.5 and 1.0, with an average value of $B \approx 0.75$ (Baines *et al.* 1990).

In order to remain consistent with the results of Baines *et al.* (1990), we use the same result for our flow in an ambient density gradient. The expression for the entrained volume flux above the ascending front is therefore $q_a = Bq_o(z_f^{1/2} - z_a^{1/2})/b_o^{1/2}$. Introducing this result into (4.7), along with the dimensionless quantities defined in (4.5), leads to the result that

$$\frac{\mathrm{d}\tilde{z}_a}{\mathrm{d}\tilde{t}} = 1 + B(\tilde{z}_f^{1/2} - \tilde{z}_a^{1/2}). \tag{4.9}$$

The rise of the fountain height is predicted using the same assumptions and method that were presented in § 3.3.3 and Appendix B for an axisymmetric fountain. The details are again given in Appendix B, with the final result that

$$\tilde{z}_{fs} = \tilde{z}_{fs}(0) + \frac{2.43^{-3}\sigma_o^*}{0.96^{-3} + 2.43^{-3}\sigma_o^*}\frac{\tilde{t}}{3}, \tag{4.10a}$$

and

$$\tilde{z}_{fh} = \tilde{z}_{fh}(0) + \tfrac{2}{3}\tilde{z}_r\tilde{t}, \tag{4.10b}$$

where $\tilde{z}_r = \tilde{z}_{fh}(0)/(\tilde{z}_{fh}(0) + \tilde{z}_e)$ (Baines *et al.* 1990), $\tilde{z}_{fs}(0)$ is the symmetric fountain height at $\tilde{t} = 0$, and $\tilde{z}_{fh}(0)$ is defined in (B 13).

Finally, the weighting function which quantifies the transition between (4.10*a*) and (4.10*b*), is again given by (3.16), with $\tilde{z}_v = 0$. It therefore follows that the final expression for the fountain height is also given by (3.17), with $\tilde{z}_{fs}$ and $\tilde{z}_{fh}$ defined by (4.10*a*) and (4.10*b*) respectively. This expression for $\tilde{z}_f$ can then be used in the numerical integration of (4.9) to find the position of the ascending front.

4.3.2. *Experimental results*

The position of the fountain height, the ascending front and the descending front were measured in three experiments in which σ^* was varied. These results are shown in figure 11, along with the predicted position of the top of the fountain, the ascending front and, where applicable, the descending front. The fountain height at $t = 0$ is found from a combination of (4.2) and (4.4*b*), while the spreading height was taken from the experimental measurements. In figures 11(*a*) and 11(*b*), the position of the descending front is well described by (4.6) until it approaches to within approximately 2 cm ($\tilde{z} \approx 430$) of the source. After this point, the environmental fluid is entrained into the initial axisymmetric flow from the holes, and consequently, the exponential decay predicted for axisymmetric flow can be observed. In figure 11(*a*), the position of the fountain height is slightly overestimated by the theoretical prediction. In contrast, in figures 11(*b*) and 11(*c*), in which the profile fluctuates significantly, (3.17) represents a good average of the measured heights. Using the average value of $B = 0.75$ in all experiments provides good predictions of the motion of the ascending front, and enables accurate estimates of the time t^* when the front reaches the height of the fountain.

4.4. *Ambient density profile*

The numerical method which was used in § 3.4 to quantify the changes to the ambient density profile can be adapted for a line fountain with few alterations. The reduction in the thickness of each layer in the density profile is found by using $q_d = (\alpha/2)^{1/2}q_0 z_d^{1/2}/b_0^{1/2}$ or $q_a = Bq_0(z_f^{1/2} - z_a^{1/2})/b_0^{1/2}$ to determine the volume of

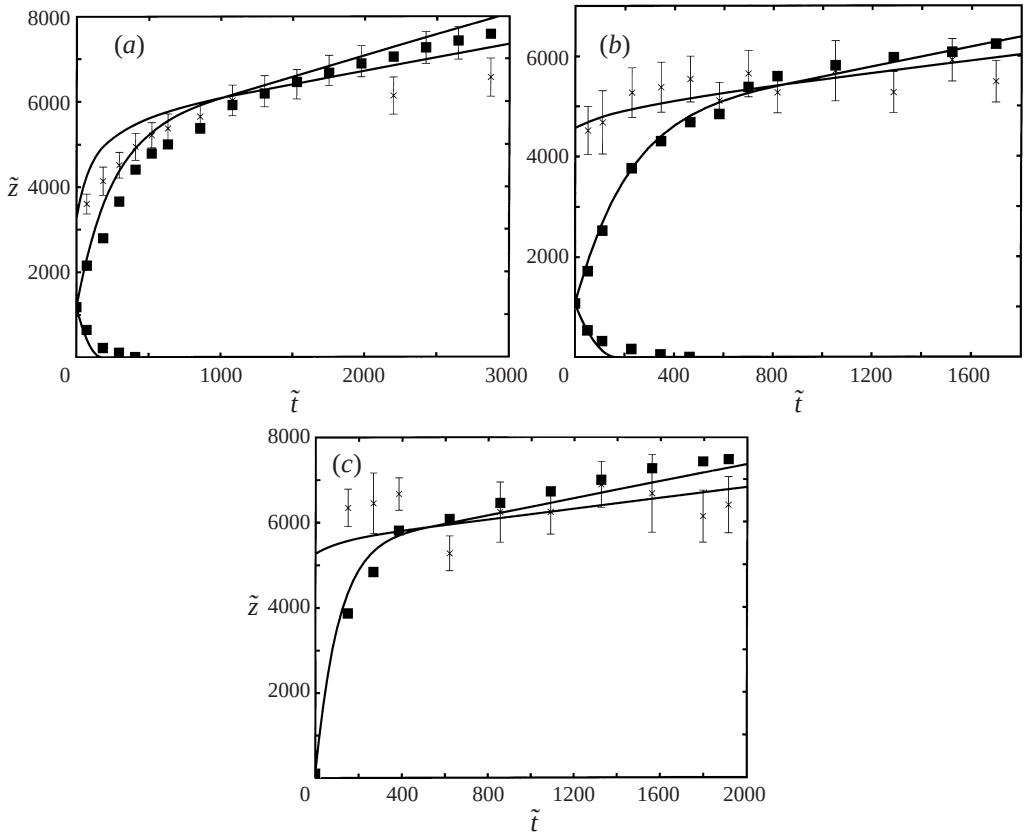

FIGURE 11. Experimental measurements of the fountain height (×) and the fronts (■) along with the theoretical predictions (solid line) for the fountain height (3.17), the ascending front (4.9) and, where applicable, the descending front (4.6): (*a*) $q_o = 2.19 \times 10^{-4}\,\mathrm{m^2\,s^{-1}}$, $N = 1.38\,\mathrm{s^{-1}}$; $\sigma^* = \infty$; (*b*) $q_o = 2.19 \times 10^{-4}\,\mathrm{m^2\,s^{-1}}$, $N = 0.71\,\mathrm{s^{-1}}$, $\Delta_o = 0.34\,\mathrm{m\,s^{-2}}$; $\sigma^* = 21$; (*c*) $q_o = 2.19 \times 10^{-4}\,\mathrm{m^2\,s^{-1}}$, $N = 0.32\,\mathrm{s^{-1}}$, $\Delta_o = 0.31\,\mathrm{m\,s^{-2}}$; $\sigma^* = 5.2$.

fluid removed in each time interval $\Delta\tilde{t}$. We therefore obtain the result that

$$\Delta\tilde{z}'_j = \Delta\tilde{z}_j - \begin{cases} (\alpha/2)^{1/2}\left((\tilde{z}_j + \Delta\tilde{z}_j)^{1/2} - \tilde{z}_j^{1/2}\right)\Delta\tilde{t}, & \tilde{z}_j < \tilde{z}_d \\ B\left((\tilde{z}_j^{1/2} + \Delta\tilde{z}_j)^{1/2} - \tilde{z}_j^{1/2}\right)\Delta\tilde{t}, & \tilde{z}_d < \tilde{z}_j < \tilde{z}_f. \end{cases} \tag{4.11}$$

It is possible in this case that for layers near the base, this calculation may result in a negative thickness. The program was therefore adapted to check for and prevent this occurring.

The fluid entrained from the layers mixes into the fountain so that the final density of the downflow at the point of intrusion is

$$\rho_m = \frac{\rho_i + (\alpha/2)^{1/2}\sum_{\tilde{z}_j=0}^{\tilde{z}_d}\rho(\tilde{z}_j)\left((\tilde{z}_j + \Delta\tilde{z}_j)^{1/2} - \tilde{z}_j^{1/2}\right) + B\sum_{\tilde{z}_j=\tilde{z}_d}^{\tilde{z}_f}\rho(\tilde{z})\left((\tilde{z}_j + \Delta\tilde{z}_j)^{1/2} - \tilde{z}_j^{1/2}\right)}{1 + (\alpha/2)^{1/2}\sum_{\tilde{z}_j=0}^{\tilde{z}_d}\left((\tilde{z}_j + \Delta\tilde{z}_j)^{1/2} - \tilde{z}_j^{1/2}\right) + B\sum_{\tilde{z}_j=\tilde{z}_d}^{\tilde{z}_f}\left((\tilde{z}_j + \Delta\tilde{z}_j)^{1/2} - \tilde{z}_j^{1/2}\right)}. \tag{4.12}$$

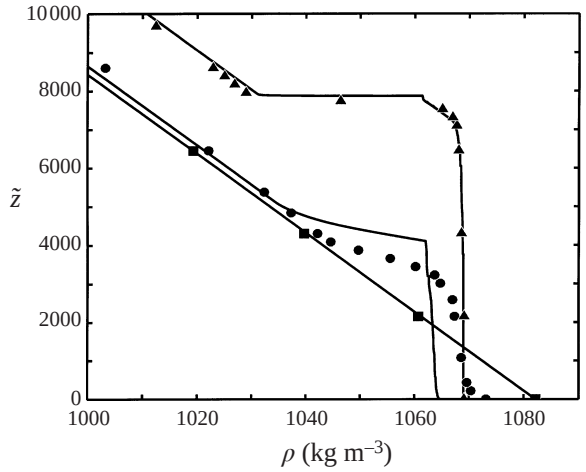

FIGURE 12. Comparison between the numerical results (solid line) and the measured ambient density profiles produced by a line fountain, with the experimental parameters listed in the caption to figure 11(*a*). Profiles were measured at $t = 0$ (■), $t = 60$ s (●) and $t = 13$ min (▲).

The new layer with this density has a thickness of

$$\Delta\tilde{z}'_n = \left(1 + (\alpha/2)^{1/2} \sum_{\tilde{z}_j=0}^{\tilde{z}_d} \left((\tilde{z}_j + \Delta\tilde{z}_j)^{1/2} - \tilde{z}_j^{1/2}\right) + B \sum_{\tilde{z}_j=\tilde{z}_d}^{\tilde{z}_f} \left((\tilde{z}_j + \Delta\tilde{z}_j)^{1/2} - \tilde{z}_j^{1/2}\right)\right)\Delta\tilde{t}. \quad (4.13)$$

Using the same procedure, initial step size and time interval described in § 3.4 for an axisymmetric fountain, the profile is then updated at each time step. An example of these numerical results is shown in comparison to the experimental measurements of a profile in figure 12. At intermediate times, the theory again predicts a more homogeneous environment than that measured experimentally. The neglect of additional mixing and density variation in the downflow again result in some difference (§ 3.4), but in the case of a line fountain, the fluctuations in the fountain profile also lead to differences between the numerical predictions and experimental measurements. At large times the agreement is seen to be good.

5. Applications

We now present three quantitative examples of how the results of this study can be applied to physical problems.

5.1. *The heating or cooling of a room*

In an enclosed room, axisymmetric turbulent fountains may arise either when hot air is forced down through the ceiling into a cold room or when cool air is forced up through the floor into a hot room. In domestic situations, it is often preferable to quickly heat or cool the lower, inhabited part of the room. The time taken for the respective fountains to heat or cool the area near the floor, as well as the resulting temperature profile, can be found using the calculations described in § 3.3 and § 3.4. In the following quantitative analysis, we assume a closed system in which air is

Heating				
T_i(°C)	σ	$z_f(0)$ (m)	Time when $z_a = 4$ m (min)	Temperature profile (°C) (floor – ceiling)
20	30	3	21	17
22	8	2.7	32	17.25–17.75
24	3	2.4	41	20–20.5
Cooling				
T_i(°C)	σ	$z_f(0)$ (m)	Time when $z_a = 2$ m (min)	Temperature profile (°C) (floor – 2 m)
20	5	2.5	6	24.9
15	1	2	9	23–25
10	0.5	1.6	14	20–23

TABLE 2. Properties of the fountain and the ambient temperature profile in the two cases of heating and cooling an initially stratified room.

removed from the room through vents on the floor (when heating) or the ceiling (when cooling) at the same rate at which the heated or cooled air is injected again through the other vent as a fountain. This positioning of the outflow vents ensures that the removal of air does not interfere with the dynamics of the fountain.

For these illustrative examples, we have considered a room 4 m high and 5 m × 5 m in area, with rectangular vents of area $A_v = 0.01\,\mathrm{m}^2$ in the floor and the ceiling. The air is injected and removed through these vents at a flow rate of $Q_o = 0.02\,\mathrm{m}^3\,\mathrm{s}^{-1}$.

5.1.1. *Heating a cold room*

To completely heat a room using warm air injected through the ceiling, the ascending front, which is moving down, must reach the floor. In this example, we consider a room in which the ambient temperature at the floor, $T_f = 14\,^\circ\mathrm{C}$, increases at a rate of $1\,^\circ\mathrm{C\,m}^{-1}$ to 18 °C at the ceiling. The buoyancy frequency is then calculated using a thermal expansion coefficient of $\beta \approx \frac{1}{300}\ \mathrm{K}^{-1}$ to be $N = 0.18\,\mathrm{s}^{-1}$. In table 2, we show the effect of varying the temperature of the injected air on both the time taken to heat the room to floor level, and the final ambient temperature. These calculations show that the floor level is heated in only 21 minutes when the injected air is only slightly warmer than the ambient at the ceiling ($T_i = 20\,^\circ\mathrm{C}$). However, this case results in a modest increase in the overall ambient room temperature to 17 °C. In contrast, if the temperature of the injected air is increased to $T_i = 24\,^\circ\mathrm{C}$, the room is heated to 20.25 °C, although the time taken is almost doubled ($t = 41$ min).

5.1.2. *Cooling a hot room*

To cool the lower regions of a room, cold air is injected upwards through the vent in the floor. In this example, the ambient temperature of $T_f = 25\,^\circ\mathrm{C}$ at the floor increases with height at a rate of $1\,^\circ\mathrm{C\,m}^{-1}$ to again give a buoyancy frequency of $N = 0.18\,\mathrm{s}^{-1}$. In this case, it is preferable that the downflow spreads along the floor to create a layer of air which is colder than that originally in the room. It was found by Bloomfield & Kerr (1998) that this condition is satisfied for $T_i < 20\,^\circ\mathrm{C}$. In table 2, we show how varying the temperature of the injected air affects the time taken to fill the room with cold air to a depth of 2 m. Also shown is the resulting temperature profile within this lower 2 m region. When the temperature of the injected air is $T_i =$

20 °C, the air in the lower 2 m of the room is mixed to a homogeneous temperature of $T = 24.9\,^{\circ}\mathrm{C}$ in only 6 min, but little cooling occurs. When the injected air has a temperature of $T_i = 10\,^{\circ}\mathrm{C}$, it takes 14 min to cool the lower 2 m to a temperature of between 20 °C at the floor and 23 °C at a height of 2 m.

5.2. *The replenishment of magma chambers*

Hot magma that rises through the Earth's crust can pond in large chambers (Campbell & Turner 1989). These chambers, which can be density stratified, can then be replenished by the inflow of magma through a fissure at their base, forming a turbulent line fountain. Our results from § 4 may be used to predict some of the main properties of the evolution of the chamber. In particular it is possible to calculate the time at which the descending front reaches the base and to estimate the time at which the ascending front passes the top of the fountain.

We consider here fissure widths of $d = 1$ m, 3 m and 10 m, and a fixed input magma density of $\rho_i = 2650\,\mathrm{kg\,m^{-3}}$. An expression for the flow rate through a fissure is given by

$$q_o = \left(\frac{g\Delta\rho}{f\rho_i}\right)^{1/2} d^{3/2}, \tag{5.1}$$

where $\Delta\rho$ is the average density difference between the input magma and the wall rocks of the fissure and f is a friction coefficient (Huppert & Sparks 1985). Probable values of $\Delta\rho = 300\,\mathrm{kg\,m^{-3}}$ and $f = 0.03$ are used here.

The size of magma chambers varies, but for these calculations we consider a large chamber 100 km in length and several kilometres deep. Within the chamber, we assume a density variation from $2640\,\mathrm{kg\,m^{-3}}$ at the floor to $2620\,\mathrm{kg\,m^{-3}}$ at the top of the stratified region, of around 1 km depth. This variation of $20\,\mathrm{kg\,m^{-3}}$ gives a buoyancy frequency of $N = 8.6 \times 10^{-3}\,\mathrm{s^{-1}}$. Above this stratified region, the density of the magma is assumed to be constant at $2620\,\mathrm{kg\,m^{-3}}$ (see Bloomfield & Kerr 1998, § 5.2, case III).

The final height of the fountain immediately after injection can be found from (4.2) and (4.4*b*), while the spreading height can be determined from the experimental results of Bloomfield & Kerr (1998). The time taken for the descending front to reach the base of the chamber is $t_d = (2z_s b_o L^2/\alpha q_o^2)^{1/2}$. To estimate t^*, the time at which the ascending front passes the top of the fountain, the same numerical computation as that performed in § 4.3.1 is required. The results of these calculations are presented in table 3. For the smallest fissure, the fountain takes the longest time ($t^* = 8$ days) to homogenize only a small region of the chamber ($z_a(t^*) = 107$ m). In contrast, for the largest fissure, it takes only 1.7 days to form a homogeneously mixed layer of depth 793 m. The evolution of the magma chamber with time for this case of the largest fissure width is shown in figure 13.

Another geologically important property of the chamber evolution is the volume ratio of magma added to magma which has accumulated in the mixed layer (table 3). When the injected and ambient magmas have different compositions (eg. olivine-saturated and plagioclase-saturated magmas), this mixing ratio is needed to determine the final composition, and hence the properties, of magma in the mixed layer. The mixing ratios of around 40% found in our calculations would result in a mixed magma which is significantly undersaturated in both olivine and plagioclase. This mixed magma would have erosive properties (Kerr 1994), leading to further evolution of the chamber and surrounding rocks.

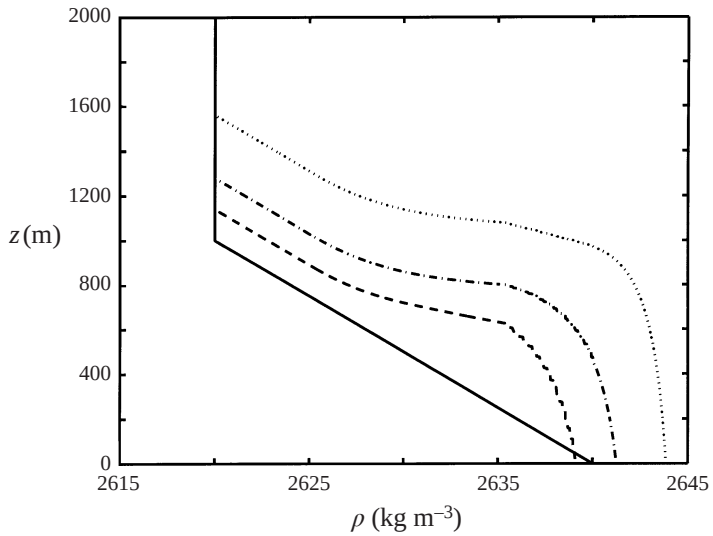

FIGURE 13. Evolution of the density profile inside a magma chamber with the properties described in §5.2 and $b_o = 5\,\mathrm{m}$. Times at which the profile is calculated are: $t = 0$ (—), $t = 0.8$ days (- -), $t = 1.7$ days (-·-·) and $t = 3.4$ days (....).

	$d = 1$ m	$d = 3$ m	$d = 10$ m
$q_o(\mathrm{m^2\,s^{-1}})$	6.1	31.6	192
σ^*	2	6	20
z_f (m)	91	257	730
z_s (m)	0	0	243
t_d (h)	0	0	26
t^* (days)	8	4.3	1.7
$z_a(t^*)$ (m)	107	298	793
volume added/volume in layer	0.39	0.40	0.35

TABLE 3. Properties of line fountains in a magma chamber.

6. Conclusions

We have presented an experimental and theoretical investigation into the evolution of turbulent axisymmetric and line fountains, and their effect on an initially stratified ambient density profile. In this study, we have expanded the previous work by Bloomfield & Kerr (1998) to show that the evolution of the fountain and the environment depends on whether intermediate or basal spreading occurs, and hence whether one or two fronts, respectively, are observed.

We have shown that the ambient density profile has little effect on the motion of the fronts. For the descending front, this assumption was verified after comparing experimental data with analytical predictions for jet-like flow. Similarly, comparison with experimental results for the ascending front lead to the conclusion that the rate of entrainment into the downflow of the fountain can be quantified using the same constant as that determined in a homogeneous fluid. The motion of the ascending front therefore depends directly on only the position of the top of the fountain. To quantify the rise of the fountain height, we first estimated the individual effects of the decreasing ambient density gradient and the increasing average ambient density.

A simple weighting function based on the thickness of the spreading layer relative to the fountain height was then used to quantify the contribution from each of these effects to the overall rise of the fountain height. A numerical solution of the equations of motion then gave the position of the fountain height and the ascending front.

For axisymmetric fountains, the theory provided an accurate prediction of the position of the fountain height and the ascending front. However, the fluctuations in the profile of a line fountain resulted in significantly more scatter of the experimental data around the average position predicted by the theory.

Once the time evolution of the axisymmetric and line fountains is known, we have shown how a simple numerical scheme can then be used to quantify the homogenization of the initially stratified environment. The results of these numerical calculations accurately predicted the changes to the ambient density distribution, particularly at later times.

Finally, we have outlined three illustrative examples of how the results of this study can be applied quantitatively to physical problems. The time evolution of a magma chamber due to the inflow of dense magma and the heating or cooling of a small room have been calculated for typical source and environmental parameters.

We thank Tony Beasley, Derek Corrigan and Ross Wylde-Browne for their technical assistance with the experiments. The financial support of an Australian Research Council Fellowship (for R. K.) and of a John Conrad Jaeger Scholarship (for L. B.) are gratefully acknowledged.

Appendix A. The timescales for lateral intrusion and vertical advection

For both axisymmetric and line fountains, the models for the motion of the fronts are valid only if the intrusion of the fluid into the environment occurs on a significantly smaller timescale than that taken for the descending front to fall to a small fraction of its initial height. In this Appendix, we determine the effect of the tank size and source conditions on these two timescales to determine the validity of our assumption of instantaneous intrusion. The following analysis applies only to the situations in which intrusion occurs at an intermediate height in the environment.

A.1. *Axisymmetric fountains*

Following the analysis presented by Cardoso & Woods (1992) for a plume in a stratified fluid, we use several simplifying assumptions to determine expressions for the dynamics of the intruding fluid. As the downflow reaches the spreading height, the flow into the intruding layer is still turbulent. However, we shall assume that the ambient stratification quickly damps this turbulence, so that little mixing occurs between the spreading layer and the environment. The dynamics of the intruding layer may then simply be described by a Froude number,

$$Fr = v/Nd, \tag{A 1}$$

where v is the horizontal velocity of the fluid in the layer and d is its thickness (figure 14). It was shown by Manins (1979) that the Froude number in the outflow is approximately constant with a lower bound of $2^{-1/2}$.

We make the assumption that the velocity of the descending front is horizontally constant and is equal to U_s. From the conservation of volume we therefore write the horizontal volume flux at a distance r from the fountain axis as

$$Q(r) = 2\pi rvd = Q_s - U_s\pi(r^2 - a_s^2), \tag{A 2}$$

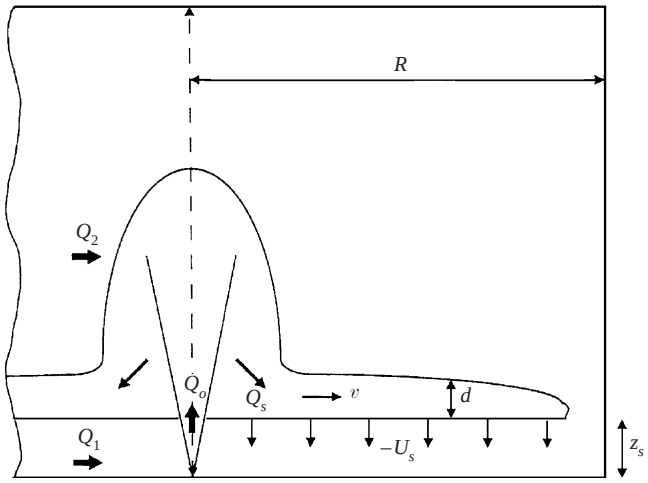

FIGURE 14. Geometry illustrating the outflow of fluid into the spreading layer.

where a_s is the fountain radius at the spreading height and Q_s is the volume flux into the intruding layer at $r = a_s$. To simplify the analysis, we consider a tank of circular cross-section with radius R, so that the area, πR^2, is equal to the area of our tank, A. As there can be no flow through the walls of the tank, $Q(R) = 0$. This result can be used to eliminate U_s from (A 2) giving

$$Q(r) = 2\pi r dv = Q_s \left(\frac{R^2 - r^2}{R^2 - a_s^2} \right). \tag{A 3}$$

Introducing (A 1) in (A 3), we find the radial dependence of d and v:

$$d = \left(\frac{Q_s}{2\pi r FrN} \left(\frac{R^2 - r^2}{R^2 - a_s^2} \right) \right)^{1/2} \tag{A 4a}$$

$$v = \left(\frac{FrNQ_s}{2\pi r} \left(\frac{R^2 - r^2}{R^2 - a_s^2} \right) \right)^{1/2}. \tag{A 4b}$$

The time taken for fluid to spread from $r = a_s$ to $r = R$ is therefore

$$t_1 = \int_{a_s}^{R} \frac{\mathrm{d}r}{v} = \left(\frac{2\pi(R^2 - a_s^2)}{FrNQ_s} \right)^{1/2} \int_{a_s}^{R} \left(\frac{r}{R^2 - r^2} \right)^{1/2} \mathrm{d}r. \tag{A 5}$$

After making the substitution $r = R \sin\theta$ and letting $a_s \to 0$, (A 5) is integrated numerically to give the same result as that obtained by Cardoso & Woods (1992):

$$t_1 = \left(\frac{4\pi R^3}{FrNQ_s} \right)^{1/2} \int_0^{\pi/2} \sin^{1/2}\theta \, \mathrm{d}\theta \approx 1.2 \left(\frac{2\pi R^3}{FrNQ_s} \right)^{1/2}. \tag{A 6}$$

The volume flux of fluid added to the spreading layer is given by

$$Q_s = Q_o + Q_1 + Q_2, \tag{A 7}$$

where $Q_1 = 2\alpha Q_o(z_s - z_v)/r_e$ is the volume flux entrained into the jet-like flow below the spreading height and $Q_2 = BQ_o(z_f - z_s)/r_e$ is the volume flux entrained into the downflow of the fountain (figure 13). The first term in (A 7) is negligible in these experiments, so that

$$Q_s \approx (Q_o/r_e)\left(2\alpha(z_s - z_v) + B(z_f - z_s)\right). \tag{A 8}$$

We chose the time taken for the position of the descending front to fall from its initial height above the base, $z_s - z_v$, to a height of $e^{-2}(z_s - z_v) \approx 0.1(z_s - z_v)$ to represent the vertical advection in the tank, t_2:

$$t_2 = (Ar_e/\alpha Q_o). \tag{A 9}$$

Using (A 8) and a value of $Fr = 2^{-1/2}$, the ratio of (A 6) to (A 9) becomes

$$(t_1/t_2) = 0.09(Q_o/Nr_eR)^{1/2}(2\alpha(z_s - z_v) + B(z_f - z_s))^{-1/2}. \tag{A 10}$$

This ratio is valid while the fluid intrudes at an intermediate height, that is for σ in the range $\sigma_c < \sigma < \infty$. For the source parameters in the experiments performed, we obtain values of $t_1/t_2 \approx 0.08$. This small value indicates that the assumption of instantaneous spreading is valid in our experiments.

A.2. *Line fountains*

A similar analysis is used to determine the timescale of lateral intrusion for a line fountain. Conservation of horizontal volume flux in the spreading layer on one side of the upflow at a distance x from the fountain axis gives

$$q(x) = dv = \tfrac{1}{2}q_s - U_s(x - a_s), \tag{A 11}$$

where q_s is the total volume flux in the outflow at the spreading height. Expressions for the thickness and velocity within the spreading layer are obtained by combining (A 1) with (A 11) under the condition that $q = 0$ at $x = L/2 = l$:

$$d = \left(\frac{q_s}{2NFr}\left(\frac{l - x}{l - a_s}\right)\right)^{1/2} \tag{A 12a}$$

$$v = \left(\frac{NFrq_s}{2}\left(\frac{l - x}{l - a_s}\right)\right)^{1/2}. \tag{A 12b}$$

The time taken for the fluid to spread from $x = a_s$ to $x = l$ is

$$t_1 = \int_{a_s}^{l} \frac{\mathrm{d}x}{v} = \left(\frac{2(l - a_s)}{NFrq_s}\right)^{1/2} \int_{a_s}^{l} \frac{\mathrm{d}x}{(l - x)^{1/2}}. \tag{A 13}$$

In the limit as $a_s \to 0$, this is integrated to give

$$t_1 = \left(\frac{8l^2}{NFrq_s}\right)^{1/2}. \tag{A 14}$$

The volume flux of fluid into the spreading layer is again given by $q_s = q_o + q_1 + q_2$ with $q_1 = (2\alpha q_o^2 z_s/b_o)^{1/2}$ and $q_2 = Bq_o(z_f^{1/2} - z_s^{1/2})/b_o^{1/2}$, so that

$$\begin{aligned} q_s &= q_o\left(1 + (2\alpha z_s/b_o)^{1/2} + B(z_f^{1/2} - z_s^{1/2})/b_o^{1/2}\right) \\ &\approx q_o\left((2\alpha z_s)^{1/2} + B(z_f^{1/2} - z_s^{1/2})\right)/b_o^{1/2}. \end{aligned} \tag{A 15}$$

A typical timescale for the vertical motion in the ambient fluid is the time taken for the descending front to reach the base of the tank:

$$t_2 = \left(8l^2 b_o z_s/\alpha q_o^2\right)^{1/2}. \tag{A 16}$$

Using (A 15) and a value of $Fr = 2^{-1/2}$, the ratio of (A 14) to (A 16) becomes

$$\frac{t_1}{t_2} = 0.32 \left(\frac{q_o}{N b_o^{1/2} z_s ((2\alpha z_s)^{1/2} + B(z_f^{1/2} - z_s^{1/2}))} \right)^{1/2}. \tag{A 17}$$

Using our experimental parameters, we obtain the result that $t_1/t_2 \approx 0.4$–0.5. The assumption of instantaneous spreading may therefore introduce some deviation between the theory and experiments. In particular, at small times, the variation in the thickness of the outflow makes it difficult to accurately measure the position of the fronts. This effect was reduced, but not eliminated, by measuring the height of the fronts close to the axis of the fountain.

Appendix B. Derivation of the expressions for the fountain height

To determine an expression for the rise of the fountain height, we quantify separately the rise due to the decreasing stratification, $z_{fs}(t)$, and the rise due to the increasing mean ambient density, $z_{fh}(t)$.

B.1. *Axisymmetric fountain height*

To quantify $z_{fs}(t)$, the average ambient density gradient over the height of the fountain is approximated by

$$\frac{\mathrm{d}\rho}{\mathrm{d}z}(t) = \frac{\rho_{z_f}(t) - \rho_o}{z_{fs} - z_v}, \tag{B 1}$$

where $\rho_{z_f}(t)$ is the ambient density at the level of the top of the fountain, which is at a height $(z_{fs} - z_v)$ above the base of the tank. At small times, a good approximation for ρ_{z_f} is obtained by assuming that all ambient density levels above the ascending front rise at the same rate as the free surface (see figure 5*b*). The position of a thin layer which is initially at a height z_o is therefore given by $z(t) = z_o + Q_o t/A$. When this layer reaches z_{fs}, $\rho_{z_f} = \rho_o + (\mathrm{d}\rho/\mathrm{d}z)|_o (z_o - z_v)$, giving

$$\rho_{z_f} = \rho_o + \left.\frac{\mathrm{d}\rho}{\mathrm{d}z}\right|_o \left(z_{fs} - z_v - \frac{Q_o t}{A} \right), \tag{B 2}$$

where $(\mathrm{d}\rho/\mathrm{d}z)|_o$ is the initial density gradient. As a first approximation for z_{fs}, we use (B 2) to quantify $\rho_{z_f}(t)$ for all times. Combining (B 1) and (B 2), we therefore obtain an expression for $N^2(t)$:

$$N^2(t) = N_o^2 \frac{z_{fs} - z_v - Q_o t/A}{z_{fs} - z_v}, \tag{B 3}$$

where N_o is the initial buoyancy frequency. Introducing (B 3) into the definition of σ, and combining (3.1) and (3.3*b*) leads to the result that

$$z_{fs} = \left(1.85^{-4} + 3.0^{-4} \sigma_o \frac{z_{fs} - z_v - Q_o t/A}{z_{fs} - z_v} \right)^{-1/4} M_o^{3/4} F_o^{-1/2}, \tag{B 4}$$

where $\sigma_o = M_o^2 N_o^2 / F_o^2$. Rearranging this expression gives the final result that

$$z_{fs} = z_{fs}(0) \left(1 - \frac{3.0^{-4} \sigma_o}{1.85^{-4} + 3.0^{-4} \sigma_o} \frac{Q_o t/A}{z_{fs} - z_v} \right)^{-1/4}. \tag{B 5}$$

The approximation that z_{fs} varies by only a small fraction of its initial value allows us to replace z_{fs} by $z_{fs}(0)$ on the right-hand side of (B 5). In terms of the dimensionless quantities defined in (3.8), and at small times (i.e. when $\tilde{t} \ll \tilde{z}_{fs}$) therefore

$$\tilde{z}_{fs} \approx \tilde{z}_{fs}(0) + \frac{3.0^{-4}\sigma_o}{1.85^{-4} + 3.0^{-4}\sigma_o}\frac{\tilde{z}_{rs}}{4}\tilde{t}, \tag{B 6}$$

where $\tilde{z}_{rs} = \tilde{z}_{fs}(0)/(\tilde{z}_{fs}(0) - \tilde{z}_v)$.

This expression gives a first correction to quantify how $\tilde{z}_{fs}$ increases from its initial value at small times. By the time any significant deviations from (B 6) arise, the environment is predominantly homogeneous, and $z_{fh}(t)$ better describes the rise of the fountain height.

An expression for $z_{fh}(t)$ is obtained by assuming that the ambient fluid below this height is homogeneously mixed, and then using (3.1) combined with (3.2*b*) to find the height to which the fountain would rise in a fluid with this density. If $\bar{\rho}_o$ is the average environmental density at $t = 0$, and the fountain reaches a height $z_{fh}(0)$ in this homogeneous fluid, then

$$\bar{\rho}_o = \rho_o + \left.\frac{\mathrm{d}\rho}{\mathrm{d}z}\right|_o \frac{(z_{fh}(0) - z_v)}{2}. \tag{B 7}$$

The initial buoyant acceleration of the source fluid is found using the definition of Baines *et al.* (1990) to be

$$\bar{\Delta}_o = \frac{g(\rho_i - \bar{\rho}_o)}{\bar{\rho}_o} = \frac{\Delta_o + N_o^2(z_{fh}(0) - z_v)/2}{1 - N_o^2(z_{fh}(0) - z_v)/(2g)}. \tag{B 8}$$

Using this definition of $\bar{\Delta}_o$ in (3.1) and (3.2*b*), we obtain an equation which can be solved numerically for $z_{fh}(0)$:

$$z_{fh}(0) = 1.85 M_o^{3/4} Q_o^{-1/2} \left(\frac{1 - N_o^2(z_{fh}(0) - z_v)/(2g)}{\Delta_o + N_o^2(z_{fh}(0) - z_v)/2}\right)^{1/2}. \tag{B 9}$$

In a homogeneous fluid, Baines *et al.* (1990) have shown both experimentally and theoretically that the fountain height rises at close to half the rate at which the free surface rises due to the inflow. If the same theoretical arguments are applied to estimate z_{fh}, then the equivalent result is

$$\tilde{z}_{fh} = \tilde{z}_{fh}(0) + \tfrac{1}{2}\tilde{z}_{rh}\tilde{t}, \tag{B 10}$$

where $\tilde{z}_{rh} = \tilde{z}_{fh}(0)/(\tilde{z}_{fh}(0) - \tilde{z}_v)$.

B.2. *Line fountain height*

The derivation of an expression for the height of a line fountain follows the same procedure as that outlined above for axisymmetric fountains. First, we quantify $z_{fs}(t)$ – the rise of the fountain height at small times due to the decrease in the average buoyancy frequency of the environment. The change in $N^2(t)$ is again given by (B 3), without the virtual source correction. Combining (B 3) with (4.2) and (4.4*b*), and using the dimensionless forms of z and t, we obtain the result that

$$\tilde{z}_{fs} = \tilde{z}_{fs}(0)\left(1 - \frac{2.43^{-3}\sigma_o^*}{0.96^{-3} + 2.43^{-3}\sigma_o^*}\frac{\tilde{t}}{\tilde{z}_{fs}}\right)^{-1/3}. \tag{B 11}$$

At small times, therefore,

$$\tilde{z}_{fs} = \tilde{z}_{fs}(0) + \frac{2.43^{-3}\sigma_o^*}{0.96^{-3} + 2.43^{-3}\sigma_o^*}\frac{\tilde{t}}{3}, \tag{B 12}$$

where $\tilde{z}_{fs}(0)$ is taken to be the dimensionless symmetric height, since the profile is predominantly symmetric at small times.

Second, to obtain an expression for the rise of the fountain due to the increasing average ambient density, $z_{fh}(t)$, we need to determine $z_{fh}(0)$. The initial buoyant acceleration of the source fluid is again given by (B 8) with $z_v = 0$, so that an implicit expression for $z_{fh}(0)$ is found from a combination of (4.2) and (4.3*b*) to be

$$z_{fh}(0) = \frac{\frac{1}{2}(0.96 + 0.77)m_o^{2/3}}{2^{1/3}b_o^{1/3}}\left(\frac{1 - N_o^2 z_{fh}(0)/(2g)}{\Delta_o + N_o^2 z_{fh}(0)/2}\right)^{2/3}. \tag{B 13}$$

In this expression, the average of the symmetric and asymmetric heights has been used, since the fountain in a homogeneous fluid continually fluctuates between a symmetric and an asymmetric profile. To quantify the fountain height at later times, we use the result that in a homogeneous fluid, the dimensionless fountain height rises at a rate given by

$$\tilde{z}_{fh} = \tilde{z}_{fh}(0) + \tfrac{2}{3}\tilde{z}_r\tilde{t}. \tag{B 14}$$

where $\tilde{z}_r = \tilde{z}_{fh}(0)/(\tilde{z}_{fh}(0) + \tilde{z}_e)$ (Baines *et al.* 1990).

REFERENCES

Baines, W. D. & Turner, J. S. 1969 Turbulent buoyant convection from a source in a confined region. *J. Fluid Mech.* **37**, 51–80.

Baines, W. D., Turner, J. S. & Campbell, I. H. 1990 Turbulent fountains in an open chamber. *J. Fluid Mech.* **212**, 557–592.

Batchelor, G. K. 1954 Heat convection and buoyancy effects in fluids. *Q. J. R. Met. Soc.* **80**, 339–358.

Bloomfield, L. J. & Kerr, R. C. 1998 Turbulent fountains in a stratified fluid. *J. Fluid Mech.* **358**, 335–356.

Campbell, I. H. & Turner, J. S. 1989 Fountains in magma chambers. *J. Petrol.* **30**, 885–923.

Cardoso, S. S. S. & Woods, A. W. 1993 Mixing by a turbulent plume in a confined stratified region. *J. Fluid Mech.* **250**, 277–305.

Crapper, P. F. 1977 A note on the characteristics of a two–dimensional jet produced by a series of co–planar three–dimensional jets. *J. Indust. Aero.* **2**, 181–183.

Germeles, A. E. 1975 Forced plumes and mixing of liquids in tanks. *J. Fluid Mech.* **71**, 601–623.

Huppert, H. E. & Sparks, R. S. J. 1985 Komatiites I: Eruption and flow. *J. Petrol.* **26**, 694–725.

Kerr, R. C. 1994 Dissolving driven by vigorous compositional convection. *J. Fluid Mech.* **280**, 287–302.

Manins, R. C. 1979 Turbulent buoyant convection from a source in a confined region. *J. Fluid Mech.* **91**, 765–781.

Morton, B. R. 1959 Forced plumes. *J. Fluid Mech.* **5**, 151–163.

Morton, B. R., Taylor, G. I. & Turner, J. S. 1956 Turbulent gravitational convection from maintained and instantaneous sources. *Proc. R. Soc. Lond.* A **234**, 1–23.

Oster, G. 1965 Density gradients. *Sci. Am.* **213**, 70–76.

Rodi, W. 1982 *Turbulent Buoyant Jets and Plumes*. Pergamon.

Turner, J. S. 1966 Jets and plumes with negative or reversing buoyancy. *J. Fluid Mech.* **26**, 779–792.

Turner, J. S. 1973 *Buoyancy Effects in Fluids*. Cambridge University Press.